ACS APPLIED MATERIALS & INTERFACES

Research Article

www.acsami.org

Three-Dimensional Nanomechanical Mapping of Amorphous and Crystalline Phase Transitions in Phase-Change Materials

Ilja Grishin,[†] Bryan D. Huey,[‡] and Oleg V. Kolosov*[,†]

[†]Physics Department, Lancaster University, Lancaster LA1 4YB, United Kingdom

[‡]Institute of Materials Science, University of Connecticut, 97 North Eagleville Rd, Storrs, Connecticut 06269, United States

Supporting Information

ABSTRACT: The nanostructure of micrometer-sized domains (bits) in phase-change materials (PCM) that undergo switching between amorphous and crystalline phases plays a key role in the performance of optical PCM-based memories. Here, we explore the dynamics of such phase transitions by mapping PCM nanostructures in three dimensions with nanoscale resolution by combining precision Ar ion beam cross-sectional polishing and nanomechanical ultrasonic force microscopy (UFM) mapping. Surface and bulk phase changes of laser written submicrometer to micrometer sized amorphous-to-crystalline (SET) and crystalline-to-amorphous (RESET) bits in chalcogenide $Ge_2Sb_2Te_5$ PCM are observed with 10−20 nm lateral and 4 nm depth resolution. UFM mapping shows that the Young's moduli of crystalline SET bits exceed the moduli of amorphous areas by 11 ± 2%, with crystalline content extending from a few nanometers to 50 nm in depth depending on the energy of the switching pulses. The RESET bits written with 50 ps pulses reveal shallower depth penetration and show 30−50 nm lateral and few nanometer vertical wavelike topography that is anticorrelated with the elastic modulus distribution. Reverse switching of amorphous RESET bits results in the full recovery of subsurface nanomechanical properties accompanied with only partial topography recovery, resulting in surface corrugations attributed to quenching. This precision sectioning and nanomechanical mapping approach could be applicable to a wide range of amorphous, nanocrystalline, and glass-forming materials for 3D nanomechanical mapping of amorphous−crystalline transitions.

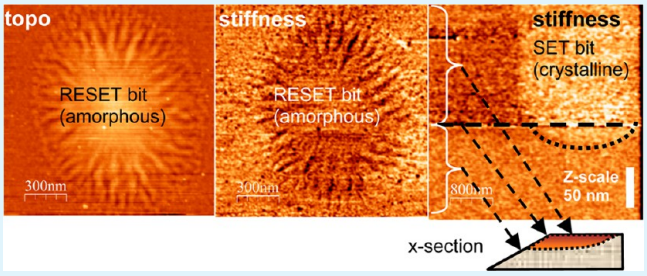

KEYWORDS: *structure−property relationships, characterization tools, nanocrystals, stimuli-responsive materials, data storage*

INTRODUCTION

Most solid-state materials, including metals, semiconductors, and insulators, can exist in amorphous and crystalline phases that exhibit radically different mechanical, optical, and electrical properties. In particular, phase-change materials (PCM)[1] exhibiting fast amorphous-to-crystalline transitions, such as GeTe-Sb_2Te_3 ternary chalcogenides,[2] are widely used in rewritable optical memory and are considered to be a promising platform for other phase-change memories.[3−6] Although the development of PCM memories requires a variety of experimental and theoretical studies,[2,7−10] it is the direct exploration of their 3D morphology and composition[8,11−13] that often provides major clues to nanoscale processes in these memory devices. Such 3D mapping requires observation of nanometer-scale features at depths up to several hundreds of nanometers, with the approaches available currently almost exclusively limited to cross-sectional transmission electron microscopy (TEM).[14−16] Moreover, amorphous-to-crystalline (SET) and crystalline-to-amorphous (RESET) transitions in nanoscale domains (bits) result in localized density changes that modify surface topography, create localized stresses, and affect mechanical properties, all of which directly influence the ultimate performance of PCM memory devices but none of which can be easily assessed by TEM. To explore amorphous−crystalline transitions in $Ge_2Sb_2Te_5$ (GST) thin films in 3D, in this article we report a recently developed versatile approach combining Ar ion beam exit cross-section polishing (BEXP) that produces nanometer flat near-surface sections[17,18] with nanomechanical ultrasonic force microscopy (UFM) mapping.[19−21] Although scanning probe microscopy (SPM) has been used before for surface topography and conductivity mapping of PCMs,[13,16,22] to the best of our knowledge the nanomechanical mapping of amorphous-to-crystalline transitions and 3D SPM studies of PCM have not been reported.

EXPERIMENTAL SECTION

PCM Films: Fabrication and Local Switching. The GST samples studied in this article were 100 nm thick films RF magnetron sputtered (Moorfield MiniLab 25) on Si and glass substrates from a stoichiometric target (Goodfellow, 99.98%), with a deposition rate of 0.35 nm s^{-1} in a process that produces a mostly amorphous layer as reported in XRD measurements elsewhere.[23] A continuous crystalline layer was produced by the annealing of as-sputtered films at 160° C on a hot plate while monitoring the reflectance change, with

Received: August 30, 2013
Accepted: October 10, 2013
Published: October 10, 2013

postannealing four-point conductivity measurements (Keithley 6430) revealing a decrease in sheet resistivity of more than 10^4-fold. The localized crystalline SET bits can be optically written by heating the sample with a focused laser beam above the crystallization temperature,[24,25] at least for a critical duration on the order of a few tens to hundreds of nanoseconds. We have used a 514 nm wavelength Ar ion laser (Spectra Physics) in continuous mode, with on-surface optical power from 1 to 30 mW. Simultaneous mechanical displacement of the sample allows narrow lines of crystalline material to be written. To write individual domains, we used mechanically chopped pulses of 200 μs in duration. Dot arrays and lines of crystalline SET bits of 500−2000 nm in size were produced in such a way on these films.

RESET amorphous bits are typically produced by local heating of the sample above the melting temperature followed by rapid cooling.[25] This requires short pulse durations on the nanosecond time scale or shorter as well as thin samples that can rapidly cool. We used 50 ps, 532 nm wavelength laser pulses from a second-harmonic Nd-YAG laser (Ekspla PL2241/50) with on-surface energies ranging from 50 to 500 pJ per pulse to write RESET bits on crystalline GST samples that were preannealed at 310 °C as the substrates. An aspherical diffraction limited lens (0.3 NA, f-11 mm) was used for laser focusing in both cases.

Three-Dimensional Cross-Sectional Polishing. A modified ion beam cutter (Leica EM TIC020) was used with the Ar ion beam directed from beneath the sample[17,18] to mill the unshielded part of the sample. This was aligned to create an obtuse angle with the intact sample surface. A 5° beam set angle resulted in a 7−11° cross-section tilt.

AFM and UFM. AFM and UFM imaging were carried out in an ambient environment (Bruker Nanoscope III, BudgetSensors ContAl-G cantilevers). UFM was performed at a 4 MHz carrier frequency and 2.7 kHz modulation frequency using sample mounting[19,21] on a 4 MHz thickness resonance piezoplate (PI) calibrated via a laser doppler vibrometer (Polytec OFV-534) (see the Supporting Information for details). The surface damage to the sample and the tip during UFM imaging is practically negligible[20] because of the effect of ultrasound-induced lubricity[26] eliminating shear forces during the scanning.

RESULTS AND DISCUSSION

Surface Nanomechanical Mapping of Phase Transitions in PCM. The topography of SET bits written by long laser pulses in the as-deposited GST film (Figure 1a) shows 2 nm depressions as a result of the higher density of the crystalline phase[13] as well as a low rms roughness of about 0.4 nm. The bit size increases with an increase in the on-surface laser power, as would be expected for long far-field-focused pulses,[10] producing, in our case, 400 nm to 2 μm bits for a power increase from 3 to 30 mW (see the example in Supporting Information Figure S1). Simultaneously acquired UFM nanomechanical images (Figure 1b) clearly show SET bits as bright (higher stiffness) areas with little contrast variation within the bit area. Given the depth probed by UFM of 2−5 nm,[27] this indicates a uniform crystalline-phase depth of at least the same thickness. By quantitatively analyzing the UFM contrast[21,27] and by considering a simplified but reasonable approximation of a "flat punch" for tip-surface contact,[28] a calibration curve can be produced (Figure 1g) (see the Supporting Information for details). Using the 110 GPa[29] Young's modulus of crystalline GST as a reference point, the Young's modulus for as-deposited amorphous regions is then 10 ± 2% lower. This result compares well with literature reports[30,31] where measurements are made by evaluation of bending of large centimeter-sized laterally and submicrometer thick PCM layers on substrates.

The morphology of amorphous (RESET) bits varied more significantly depending on the laser pulse energy. In particular,

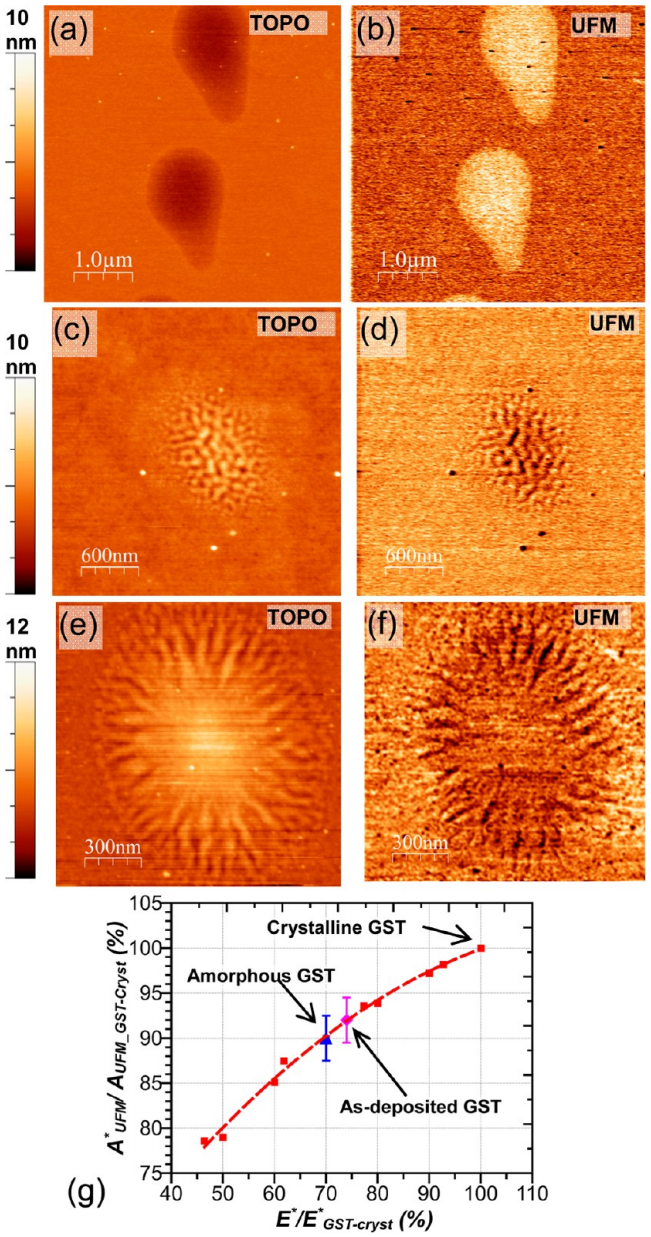

Figure 1. (a) AFM topography and (b) UFM nanomechanical map of a crystalline (SET) bit written in an amorphous as-deposited GST layer. (c, e) Topography and (d, f) UFM images of an amorphous (RESET) bit in preannealed crystalline matrix at (c, d) low and (e, f) high pulse energy. (g) Calibration curve of UFM nanomechanical response (dots and fitted dashed line). The vertical axis is the ratio of the local UFM signal to one of fully crystalline GST, and the horizontal axis is the ratio of the local effective Young's modulus (E^*) to the effective modulus of crystalline GST ($E^*_{GST-cryst}$).

the surface topography of RESET bits produced by lower pulse energies (50−100 pJ, pulse duration 30 ps, referred to here as type 1 RESET bits) generally had an elliptical shape with 2−4 nm high topographical corrugations resembling frozen "waves" (Figure 1c) with no observable average height change. The UFM nanomechanical maps, however, indicated a decreased stiffness of the bit compared with the crystalline surroundings (Figure 1d). This suggests a thin, 2−5 nm near-surface nonuniformly amorphized area, corresponding to TEM observations elsewhere.[32] Increasing the RESET bit write energy to 200−300 pJ resulted in smoother central bit areas

with a clear increase of the average height in topography (Figure 1e) (referred to as type 2 RESET domains) surrounded by topographic and mechanical waves similar to the type 1 bits (Figure 1f). Their height increase is consistent with a thicker amorphous layer because the UFM image (Figure 1f) indicates a lower elastic moduli within the bit area as well as wavelike variations of mechanical properties at the bit periphery. In both type 1 and type 2 bits, the wavelike topographic protrusions seem to be linked with the local stiffness modulation (Figure 1c,e), an observation that is studied and discussed in more detail below by investigating the 3D structure of SET–RESET–SET switched domains.

Three-Dimensional Nanomechanical Mapping. To study the 3D morphology and nanomechanics of PCM, BEXP was uniquely implemented on the basis of nonreactive, variable-energy Ar ion material removal resulting from sputtering at a glancing angle from the side of the sample below the surface line.[17,18] This produced a neat 5–10° tilted section with subnanometer roughness exhibiting minimal artifacts directly adjacent to the original surface, forming close to open-angle facets. Such geometry makes BEXP perfectly suited for SPM mapping of the surface and subsurface nanoscale morphology and physical properties of nanostructures within a single image. The low angle tilt additionally expands the depth section, enabling subsurface measurements comparable with TEM precision.[17,18] In this study, during BEXP sectioning, we investigated continuous lines of switched domains that do not require precise lateral positioning of the cut, although single bits can be also studied via a repeated BEXP process and AFM monitoring to ensure that the cut intersects a specifically desired bit.

The features of the surface part of the SET bit (above dotted lines in Figure 1a,b), namely, a depression in the topographical image in Figure 2a and the enhanced stiffness in Figure 2b, are similar to the topography and stiffness changes reported in Figure 1a,b. As anticipated, the corresponding sloped BEXP region below the sketched dotted lines in Figure 2a,b, revealing subsurface features, does not have any topographical contrast. However, it clearly shows a stiffness increase with a lenslike geometry extending as deep as 30 ± 10 nm beneath the surface (Figure 2b). Note that a separate y scale is given in Figure 2b,f for the lower parts of the images in panels a, b, e, and f, with the bar indicating the distance corresponding to 50 nm in depth given the 11 ± 0.2° BEXP polishing angle. Overall, panels a, b, e, and f therefore map topography and particularly nanomechanical contrast to as deep as several hundreds of nanometers.

The surface (i.e., above the dashed lines) of type 2 RESET bits exhibits height variations (Figure 2e) similar to those observed in Figure 1e. A clearly observed stiffness decrease is also observed in both cases (Figure 2f). The topographically flat BEXP section below the dotted line (Figure 2e), is again featureless, as expected. The corresponding UFM image (Figure 2f) reveals a less stiff amorphous zone extending into the film by approximately 50 nm. We note that subsurface nanomechanical changes for low-power SET and type 1 RESET bits are notably shallower (~5 nm or less), indicating a strong dependence of the 3D bit morphology on the switching power and energy.

Effect of Switching Conditions for SET and RESET Domains. The temperature difference, ΔT, across the GST film resulting from a long 200 μs SET pulse can be estimated using a stationary heat propagation approximation. (See the Supporting Information for a detailed analysis of the 3D temperature distribution during laser heating in these nanostructures.) These calculations estimate that for a 1.5 μm spot size at 20 mW laser power, the surface temperature will reach ~1300 °C, which should almost linearly decrease to the ambient temperature at the film–substrate interface. Such a distribution would result in annealing of a significant portion of the film depth during a long laser pulse. Using Weidenhof's[33] temperature–time relations, the crystallization temperature corresponding to a 200 μs incubation time is found to be 583 K. Using 3D finite element (FE) simulations of the temperature distribution created by the diffraction-limited Gaussian beam, we find that the 580 K crystallization isosurface is at approximately 25 nm in depth (Figure 2c), in good agreement with the experimentally measured SET bit depth via BEXP and UFM (Figure 2b). Furthermore, assuming a 6% density increase[13] during crystallization, the SET bit surface should be depressed by ~1.5 nm, also in good agreement with the experimentally observed 2 nm depressions.

For much shorter RESET bit pulse, time-dependent heat propagation was used (see the Supporting Information) with FE analysis, producing a temperature distribution on the axis of

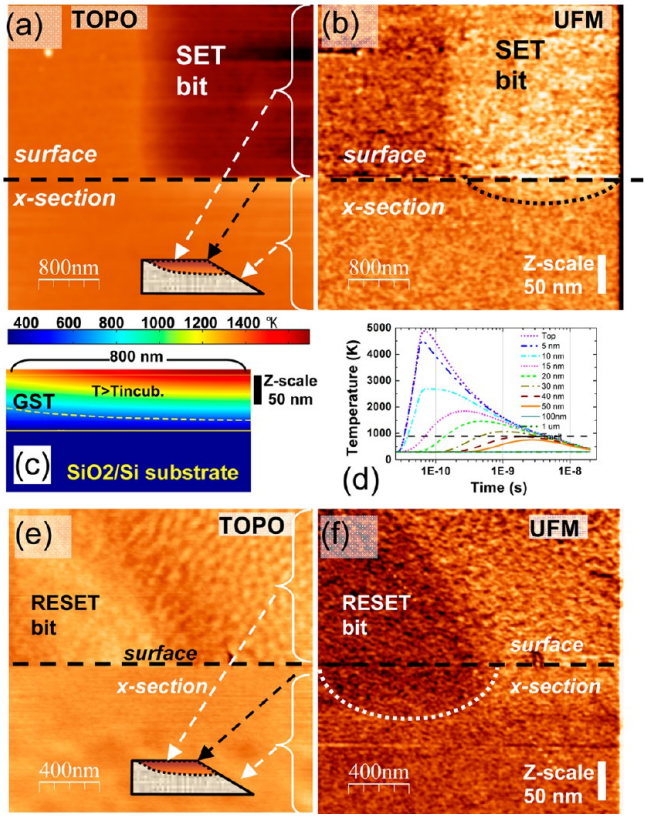

Figure 2. (a) AFM and (b) UFM stiffness image of the surface (top half, above dashed line) and BEXP cross-section (bottom half) of the SET bit. (c) Finite elements (FE) simulation of the temperature distribution across the GST film on a Si substrate upon exposure to a 25 mW laser, where the dashed line indicates the crystallization (SET transition) temperature. (d) FE simulation of the transient temperature, T, distribution in a 100 nm GST film on a Si substrate showing $T(t)$ for several depth values on the beam axis (dashed baseline represents a melting (RESET transition) temperature). (e) AFM and (f) UFM images of a type 2 RESET bit written with high pulse energy (type 2). The z scale bar in the images in panels b and f in the cross-section area corresponds to 50 nm depth.

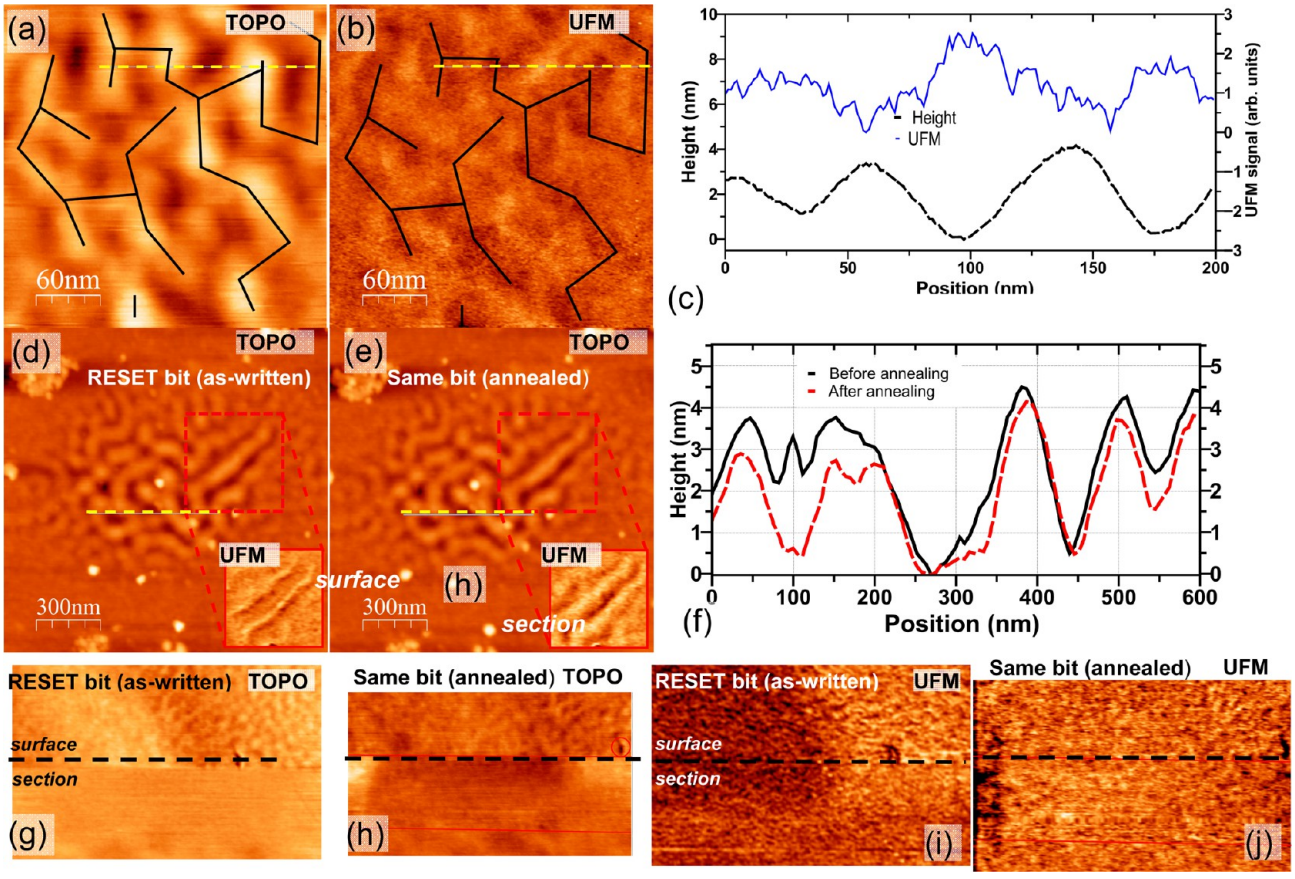

Figure 3. (a) AFM topography (z range, 3 nm) and (b) UFM nanomechanical maps of waves in a type 1 RESET bit (a ~1 nm "supersharp" AFM tip was used) and (c) corresponding 1D profiles. (d) AFM topography of as-written type 1 RESET bit (z range, 4 nm) (insets, UFM image) and (e) corresponding images of the same bit after annealing (SET state). (f) Comparison of 1D (d, f) topography profiles along dashed lines. (i) AFM and (j) UFM image of a section of a RESET type 2 bit after annealing compared with (g, h) the same bit in the as-written RESET state.

the laser beam that is plotted in Figure 2d as a function of time for the typical pulse energy of 200 pJ. The temperature that causes melting of the GST (~800 °C) is mostly confined within the top 30−40 nm of the crystalline film. The in-depth penetration of BEXP observed RESET bit lines, while being of the same order (~50 nm), is nevertheless larger than expected, possibly suggesting either multiple pulse amorphization of overlapping RESET bits along the bit line or alternative mechanisms that can cause amorphisation at lower temperatures.[3]

Surface and 3D Nanomechanical Changes of PCM during Complete SET−RESET−SET Transition Cycle. To understand the wavelike structures in RESET bits, we first compared their topography and UFM stiffness maps. As seen in Figure 3a−c, these features are clearly counter-correlated, suggesting that the crests of the topographic waves have an increased amorphous-phase content. We performed ex situ annealing of RESET bits at 310 °C, which switched them back to the crystalline SET state, and then reinvestigated the same identical bits (Figure 3d,e). Surprisingly, we found that the topography of the waves was not restored to the original flat surface, but "flattened" by only 10 to 30% (Figure 3f). Although nanomechanical contrast had changed more, some residual contrast also still remained (insets in Figure 3d,e), suggesting a degree of irreversible density and mechanical changes during the SET−RESET−SET cycle for type 1 domains produces by low-power laser pulses.

Reversing type 2 (high power) amorphous RESET bits to SET states through annealing, however, revealed that the initial topographical bulge (Figure 3g) was almost completely removed at the same location by the annealing process (Figure 3i). Only fine wave fringes similar to type 1 bits were topographically preserved. Meanwhile, the UFM nanomechanical contrast for such annealed crystalline SET bits was fully recovered (Figure 3j) as compared to their as-written type 1 RESET state (Figure 3h) . This leads to the conclusion that the observed RESET bits waves should result predominantly from a geometrical surface corrugation frozen-in during melt-quenching, with corresponding modifications of the local nanomechanical properties, whereas bulk changes of type 2 bits present true RESET phase changes.

■ CONCLUSIONS

We report direct 3D evidence of nanomechanical changes during amorphous-to-crystalline and crystalline-to-amorphous transitions in GST phase-change materials. In particular, the combination of UFM nanomechanical mapping and BEXP nano-cross-sectioning allowed novel investigations into the detailed nanoscale 3D morphology of laser-written SET and RESET bits. We were able to differentiate between permanent and reversible structural changes as well as to analyze the penetration depth of SET and RESET transitions. For SET and RESET bits written with higher power, surface topography, nanomechanical properties, and 3D structure were close to that predicted by heat propagation. Fifty-nanometer-scale wavelike

surface structures in RESET bits were also observed, attributed to a frozen-in geometry of the melt-quenching transition. This 3D nanomechanical BEXP−UFM approach therefore provides previously inaccessible insight, especially subsurface, into amorphous−crystalline phase transitions applicable to a broad range of materials and nanostructures.

■ ASSOCIATED CONTENT

Supporting Information

Quantitative analysis of nanomechanical mapping of solid state materials via UFM; BEXP cross-sectioning of PCM versus Si substrate; 3D analysis of temperature distribution during local-heating-induced phase transitions. This material is available free of charge via the Internet at http://pubs.acs.org.

■ AUTHOR INFORMATION

Corresponding Author

*Tel: +44-1524-593619. E-mail: o.kolosov@lancaster.ac.uk. Online: http://www.nano-science.com.

Notes

The authors declare no competing financial interest.

■ ACKNOWLEDGMENTS

Support from EPSRC grant EP/G015570/1, EPSRC-NSF grant EP/G06556X/1, and EU FP7 grant GRENADA (GA-246073) as well as Lancaster University research grants is acknowledged.

■ REFERENCES

(1) Ovshinsky, S. R. *Phys. Rev. Lett.* **1968**, *21*, 1450−1453.
(2) Akola, J.; Jones, R. O. *Phys. Rev. B* **2007**, *76*, 235201-1−235201-10.
(3) Burr, G. W.; Breitwisch, M. J.; Franceschini, M.; Garetto, D.; Gopalakrishnan, K.; Jackson, B.; Kurdi, B.; Lam, C.; Lastras, L. A.; Padilla, A.; Rajendran, B.; Raoux, S.; Shenoy, R. S. *J. Vac. Sci. Technol., B* **2010**, *28*, 223−262.
(4) Zhu, H.; Yin, J. A.; Xia, Y. D.; Liu, Z. G. *Appl. Phys. Lett.* **2010**, *97*, 083504-1−083504-3.
(5) Lu, Y.; Song, S.; Gong, Y.; Song, Z.; Rao, F.; Wu, L.; Liu, B.; Yao, D. *Appl. Phys. Lett.* **2011**, *99*, 243111-1−243111-3.
(6) Wang, W. J.; Shi, L. P.; Zhao, R.; Lim, K. G.; Lee, H. K.; Chong, T. C.; Wu, Y. H. *Appl. Phys. Lett.* **2008**, *93*, 043121-1−043121-3.
(7) Welnic, W.; Pamungkas, A.; Detemple, R.; Steimer, C.; Blugel, S.; Wuttig, M. *Nat. Mater.* **2006**, *5*, 56−62.
(8) Lyeo, H. K.; Cahill, D. G.; Lee, B. S.; Abelson, J. R.; Kwon, M. H.; Kim, K. B.; Bishop, S. G.; Cheong, B. K. *Appl. Phys. Lett.* **2006**, *89*, 151904-1−151904-3.
(9) Bhaskaran, H.; Sebastian, A.; Pauza, A.; Pozidis, H.; Despont, M. *Rev. Sci. Instrum.* **2009**, *80*, 083701-1−083701-6.
(10) Chang, C. M.; Chu, C. H.; Tseng, M. L.; Chiang, H. P.; Mansuripur, M.; Tsai, D. P. *Opt. Express* **2011**, *19*, 9492−9504.
(11) Wong, H. S. P.; Raoux, S.; Kim, S.; Liang, J. L.; Reifenberg, J. P.; Rajendran, B.; Asheghi, M.; Goodson, K. E. *Proc. IEEE* **2010**, *98*, 2201−2227.
(12) Raoux, S.; Rettner, C. T.; Jordan-Sweet, J. L.; Kellock, A. J.; Topuria, T.; Rice, P. M.; Miller, D. C. *J. Appl. Phys.* **2007**, *102*, 094305-1−094305-8.
(13) Do, K.; Lee, D.; Ko, D. H.; Sohn, H.; Cho, M. H. *Electrochem. Solid-State Lett.* **2010**, *13*, 284−286.
(14) Krusin-Elbaum, L.; Cabral, C.; Chen, K. N.; Copel, M.; Abraham, D. W.; Reuter, K. B.; Rossnagel, S. M.; Bruley, J.; Deline, V. R. *Appl. Phys. Lett.* **2007**, *90*, 141902-1−141902-3.
(15) Libera, M.; Chen, M. *J. Appl. Phys.* **1993**, *73*, 2272−2282.
(16) Kim, J.; Kwon, M. H.; Song, K. B. *Ultramicroscopy* **2008**, *108*, 1246−1250.
(17) Kolosov, O. V.; Grishin, I.; Jones, R. *Nanotechnology* **2011**, *22*, 8.
(18) Robson, A.; Grishin, I.; Young, R.; Sanchez, A. M.; Kolosov, O.; Hayne, M. *ACS Appl. Mater. Interfaces* **2013**, 3241−3245.
(19) Kolosov, O. V.; Yamanaka, K. *Jpn. J. Appl. Phys., Part 2* **1993**, *32*, 1095−1098.
(20) Dinelli, F.; Albonetti, C.; Kolosov, O. V. *Ultramicroscopy* **2011**, *111*, 267−272.
(21) Dinelli, F.; Assender, H. E.; Takeda, N.; Briggs, G. A. D.; Kolosov, O. V. *Surf. Interface Anal.* **1999**, *27*, 562−567.
(22) Welnic, W.; Kalb, J. A.; Wamwangi, D.; Steimer, C.; Wuttig, M. *J. Mater. Res.* **2007**, *22*, 2368−2375.
(23) Park, S. J.; Jang, M. H.; Park, S.-J.; Cho, M.-H.; Ko, D.-H. *Appl. Surf. Sci.* **2012**, *258*, 9786−9791.
(24) Wuttig, M.; Yamada, N. *Nat. Mater.* **2007**, *6*, 824−832.
(25) Kolobov, A. V.; Fons, P.; Frenkel, A. I.; Ankudinov, A. L.; Tominaga, J.; Uruga, T. *Nat. Mater.* **2004**, *3*, 703−708.
(26) Dinelli, F.; Biswas, S. K.; Briggs, G. A. D.; Kolosov, O. V. *Appl. Phys. Lett.* **1997**, *71*, 1177−1179.
(27) McGuigan, A. P.; Huey, B. D.; Briggs, G. A. D.; Kolosov, O. V.; Tsukahara, Y.; Yanaka, M. *Appl. Phys. Lett.* **2002**, *80*, 1180−1182.
(28) Dinelli, F.; Biswas, S. K.; Briggs, G. A. D.; Kolosov, O. V. *Phys. Rev. B* **2000**, *61*, 13995−14006.
(29) Jong, C. A.; Fang, W. L.; Lee, C. M.; Chin, T. S. *Jpn. J. Appl. Phys., Part 1* **2001**, *40*, 3320−3325.
(30) Kalb, J.; Spaepen, F.; Pedersen, T. P. L.; Wuttig, M. *J. Appl. Phys.* **2003**, *94*, 4908−4912.
(31) Park, I.-M.; Jung, J.-K.; Ryu, S.-O.; Choi, K.-J.; Yu, B.-G.; Park, Y.-B.; Han, S. M.; Joo, Y.-C. *Thin Solid Films* **2008**, *517*, 848−852.
(32) Meister, S.; Kim, S.; Cha, J. J.; Wong, H. S. P.; Cui, Y. *ACS Nano* **2011**, *5*, 2742−2748.
(33) Weidenhof, V.; Friedrich, I.; Ziegler, S.; Wuttig, M. *J. Appl. Phys.* **2001**, *89*, 3168−3176.